Malaysian Journal of Chemistry, 2020, Vol. 22(3), 41-51
(Special Issue: *International Conference in Organic Synthesis - ICOS 2019, Universiti Teknologi MARA*)

Synthesis, Characterization and Corrosion Inhibition Screening of Benzohydroxamic Acid Derivatives in H_2SO_4: A Langmuir Isotherm

Fatin Nurzarifah Razali, Nurul Ain Nadirah Jamaluddin and Nur Nadia Dzulkifli*
School of Chemistry and Environment, Faculty of Applied Sciences
Universiti Technologi Mara, Negeri Sembilan Branch, Kuala Pilah Campus,
72000 Kuala Pilah, Negeri Sembilan, Malaysia
*Corresponding author (e-mail: nurnadia@uitm.edu.my)

Mild steel plays an important role in many construction industries due to its low cost and outstanding mechanical properties. However, the utilization of strong acid in pickling, construction operation, and oil refining processes adds to a serious corrosion issue on mild steel. 4-nitrobenzohydroxamic acid (4NBHA) and 4-chlorobenzohydroxamic acid (4CBHA) ligands were synthesized to scrutinize the corrosion resistance activity toward mild steel in an acidic medium. Both ligands were characterized by using melting point and Fourier Transform Infrared (FTIR), ultraviolet-visible (UV-Vis) and Nuclear Magnetic Resonance (NMR) spectroscopies. The corrosion resistance of mild steel was studied with different inhibitor concentrations (1 mM, 2 mM, 3 mM, 4 mM, and 5 mM). Results of weight loss method showed that the higher the inhibitor concentration, the lower the corrosion rate. 4CBHA showed a superior corrosion resistance (%E: 80.76) due to the presence of withdrawing groups, which were the chloro group that was less reactive as compared to the nitro- group in 4NBHA (%E: 77.60). Langmuir isotherm calculation showed that the ligands were adsorbed on the mild steel surface by forming a monolayer and there were no interactions between the adsorbed inhibitors. The values of standard free energy (ΔG) were -29.36 kJ mol^{-1} for 4NBHA and -28.85 kJ mol^{-1} for 4CBHA, which indicated that both ligands were adsorbed spontaneously by chemisorption onto the metal surface by coordinate covalent bonds. Field emission scanning electron microscope (FESEM) analysis proved that the presence of a protective layer on the mild steel had restricted the corrosion process.

Key words: Benzohydroxamic acid; corrosion; Langmuir isotherm

Received: December 2019; Accepted: May 2020

Hydroxamic acid (RC(O)N(OH)R') is an organic compound which consists of a carbonyl functional group, while R and R' represent alkyl substituents. It also contains an amide (RC (O)NHR') which is the OH substitute at the NH center, as shown in Figure 1.

Corrosion is a disastrous phenomenon which causes harm to the surface of metal [1]. Corrosion occurs because of catastrophic attack on metal due to a heterogeneous chemical reaction which allows metal to develop into a chemically stable state by forming oxide, sulphide or hydroxide ions [2]. Corrosion problems which usually exist in many industries have developed huge monetary losses in terms of repair and replacement. Corrosion prevention is one of the simplest methods that can be practiced to restrain the corrosion rate in an acidic medium by developing a protective barrier against the corrosive agents.

Hydroxamic acid is advantageous in corrosion resistance activity. The nitrogen atom in hydroxamic acid is accountable for enhancing the corrosion resistance efficiency [3].

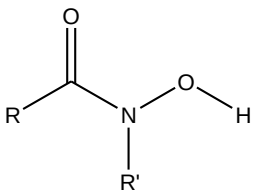

Figure 1. A general structure of hydroxamic acid

†Paper presented at the International Conference in Organic Synthesis (ICOS 2019), 9-10 December 2019, Universiti Teknologi MARA.

In this study, two types of hydroxamic acids, 4-chlorobenzohydroxamic acid (4CBHA) and 4-nitrobenzohydroxamic acid (4NBHA), were synthesized to regulate the corrosion resistance activity of the ligands in 1 M sulphuric acid solution. The objective of this study was to synthesize and characterize benzohydroxamic acid derivatives by using melting point analysis, Fourier transform infrared-attenuated total reflectance (FTIR-ATR), ultraviolet-visible (UV-Vis) and nuclear magnetic resonance (NMR) spectroscopies, and field emission scanning electron microscope (FESEM). Besides, the resistance properties of the ligands were evaluated through weight loss method, Langmuir Isotherm, and standard free energy (ΔG).

MATERIALS AND METHODS

1. Instrumentation

The infrared spectra were recorded by using mid-infrared FTIR-ATR Perkin Elmer GX spectrophotometer in the range of 4000 cm^{-1}– 650 cm^{-1}. The electronic absorption spectra were studied by using UV-Vis PG Instruments T80/T80+ spectrophotometer in the range of 200 – 600 nm with DMSO as solvent. The concentration of the samples used was 1×10^{-5} M. The ^{1}H and ^{13}C-NMR spectra were obtained by using NMR spectroscopy. The surface morphology of mild steel was observed by using A ZEISS MERLIN Compact microscope equipped with a field emission gun.

2. Synthesis of Ligands

4-nitrobenzoylchloride (4NBHA) was added dropwise into a solution of hydroxylamine hydrochloride in the presence of sodium hydrogen carbonate as catalyst for 1 h. The solution was filtered and the volume of the remaining filtrate was reduced using a rotary evaporator. Later, the solution was dissolved in ethyl acetate for precipitation. Lastly, the precipitate was filtered and dried in a desiccator. All synthesis processes were done below 4°C. The steps were repeated by using 4-chlorobenzoyl chloride (4CBHA) as the starting material.

3. Preparation of Solutions

1 M H_2SO_4 was prepared through a dilution process by using the following formula,

$$M = \frac{\frac{w}{w} x\ density\ x\ 1000}{molar\ mass} \quad \text{and} \quad McVc = MdVd$$

5 mL of 1 M H_2SO_4 was mixed with 5 mL of five different 4NBHA solution concentrations (0.001 M, 0.002 M, 0.003 M, 0.004 M, and 0.005 M) to produce the media for immersion. The process was repeated by using 4CBHA.

4. Gravimetric Method

As for mass deficit study, a mild steel was cut into pieces of the dimension of 1.5 cm × 2.5 cm. Then, the mild steel surface was polished with an emery paper to remove all sprinkled tiny particles and impurities. Next, the pieces were cleaned with distilled water and left to dry completely at room temperature. The initial mass of the mild steel pieces was recorded by using an analytical balance. The mild steel was immersed in five different media with different concentrations (0.001 M, 0.002 M, 0.003 M, 0.004 M and 0.005 M) of each inhibitor and a blank (1 M H_2SO_4), which were prepared at room temperature, for 24 h. Then, the mild steel was rinsed with distilled water and dried in a desiccator. The final mass of mild steel was measured and recorded.

RESULTS AND DISCUSSION

1. Physical Properties

The structures of 4NBHA and 4CBHA and the physical properties are shown in Figure 2, Figure 3, and Table 1, respectively.

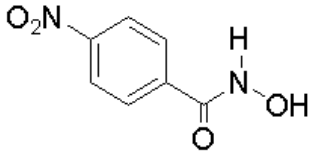

Figure 2. Proposed structure of 4NBHA

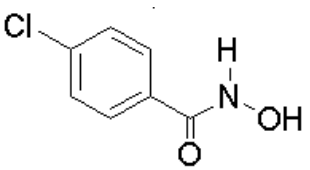

Figure 3. Proposed structure of 4CBHA

Table 1. Physical properties of ligands

Compound	Color	Melting point (°C)	Percentage yield (%)
4NBHA	White	103-105	77.75
4CBHA	White	105-107	75.48

Table 2. FT-IR values with assignments for the ligands

Compound	**Wavenumber, cm^{-1}**							
	υ(C=O)	**υ(C-NO_2)**	**υ(C-Cl) aryl chloride**	**υ(C-N) (amide)**	**υ(N-H)**	**υ(C=C) (aromatic)**	**υ(O-H)**	**υ(C-Cl)**
4-nitrobenzoyl chloride	1688	1539, 1350		1425	-	1606, 1489	-	701
hydroxylamine hydrochloride	-	-		-	3001	-	3063	-
4NBHA	1690	1538, 1349		1431	3006	1605, 1482	3395	-
4-chlorobenzoyl chloride	1775	-	1091	1400	-	1589, 1484	-	720
hydroxylamine hydrochloride	-	-	-	-	3001	-	3063	-
4CBHA	1578	-	1161	1473	2916	1506, 1480	3003	-

2. FT-IR Spectra

Some of the important infrared stretching bands in the FT-IR spectra of 4NBHA and 4CBHA are shown in Table 2.

The stretching bands of υ(C=O) that appeared at 1690 cm^{-1} (4NBHA) and 1578 cm^{-1} (4CBHA) proved the presence of ketone in the ligands [4]. Opposite to the starting materials, which were 4-nitrobenzoyl chloride and 4-chlorobenzoyl chloride, where the stretching bands were present at 1688 cm^{-1} and 1775 cm^{-1}, respectively. Therefore, the peak had a weak shift between the starting material and 4NBHA because of the presence of hydrogen bonding [5]. Besides, the conjugation effect of a carbonyl played an important role on the resonance frequency in 4CBHA. This weakened the C=O bond and the shift resulted in a lower wavenumber. Naqeebullah *et al.* (2013) [6] reported that the presence of hydroxyl group in 4NBHA and 4CBHA was due to the existence of OH from the starting material, which was hydroxylamine hydrochloride. From the 4NBHA and 4CBHA spectra, υ(O-H) stretching bands were observed at 3395 cm^{-1} and 3003 cm^{-1}, respectively. The presence of a broad band, υ(O-H) indicated the presence of extensive intramolecular hydrogen bonding between C=O and O-H. The spectra of 4NBHA and 4CBHA showed the presence of υ(C-N), which originated from both starting materials, as tabulated in Table 2. The υ(C-N) stretching band appeared as a sharp peak in the range of 1400 cm^{-1}–1473 cm^{-1} and proved that 4NBHA and 4CBHA existed as a keto form in solid state [6]. According to Sandeep and Suryaprakash (2017) [7], the nitro group (NO_2) was presented as two strong absorptions near 1550 cm^{-1} and 1350 cm^{-1}. Two strong stretching bands were displayed at 1539 cm^{-1} and 1350 cm^{-1} for 4-nitrobenzoylchloride, while 1538 cm^{-1} and 1349 cm^{-1} for 4NBHA. The effect of a conjugation of nitro group at para position in the aromatic ring caused the stretching bands to shift to the lower frequencies. 4CBHA showed the existence of υ(C-Cl), aryl chloride, at 1161 cm^{-1} and 4-chlorobenzoyl chloride at 1090 cm^{-1}. Sandeep and Suryaprakash (2017) [7] stated that aryl chloride was absorbed near 1100 cm^{-1} but 4CBHA was shifted to a higher frequency as compared to its starting material because of the electron conjugation effect at para position.

3. UV-Vis Spectra

The absorption peaks for 4NBHA and 4CBHA, as shown in Figures 4 and 5, respectively, were determined in DMSO with the concentration of 1×10^{-5} M and wavelength range of between 200 nm and 700 nm. Table 3 shows the electronic spectra data for 4NBHA and 4CBHA.

From Figures 4 and 5, intense absorption peaks for the ligands appeared at 270 nm (4NBHA) and 258 nm (4CBHA), which implied the $\pi \rightarrow \pi^*$ transition to affirm the presence of an aromatic ring in the structure [8].

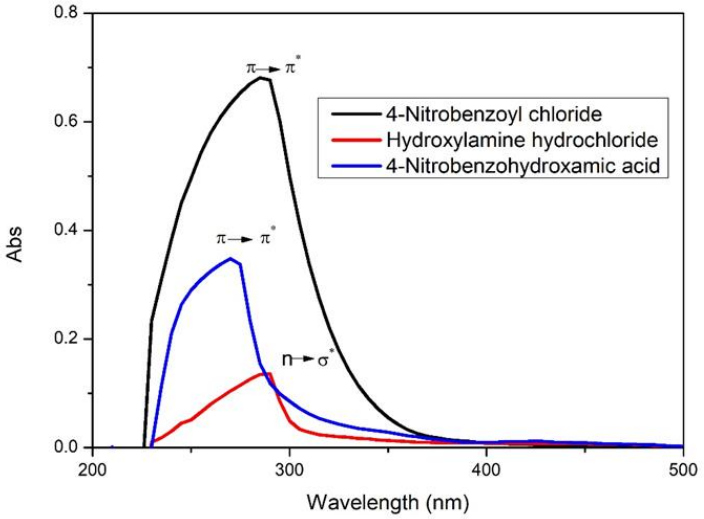

Figure 4. UV-Vis absorption spectra (1×10^{-5} M) of 4NBHA

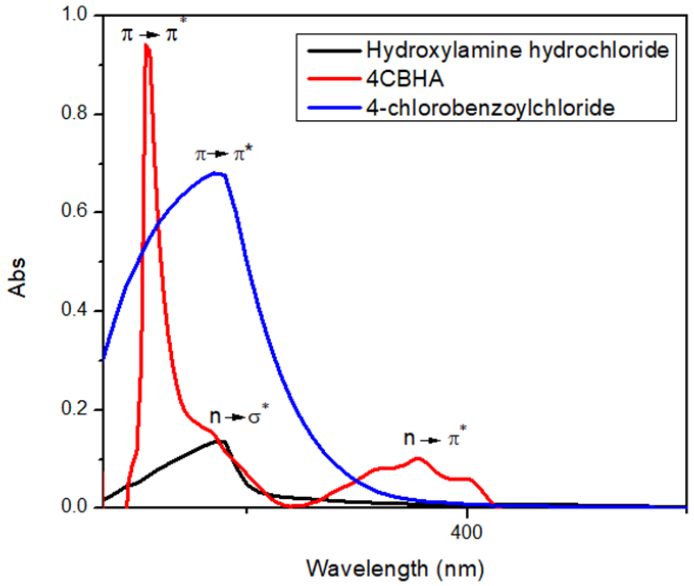

Figure 5. UV-Vis absorption spectra (1×10^{-5} M) of 4CBHA

Table 3. Electronic spectra data for 4NBHA and 4CBHA

Compound	Transition	Maximum wavelength (nm)	Molar absorptivity,ε (M^{-1} cm^{-1})
4-nitrobenzoyl chloride	$\pi \rightarrow \pi^*$	285	68100
Hydroxylamine hydrochloride	$n \rightarrow \sigma^*$	290	13600
4NBHA	$\pi \rightarrow \pi^*$	270	34800
4-chlorobenzoyl chloride	$\pi \rightarrow \pi^*$	287	66100
4CBHA	$\pi \rightarrow \pi^*$	258	95000
	$n \rightarrow \pi^*$	379	1100

Table 4. NMR data of ligands

Spectrum	Signal position(ppm)	Compound	Structure
^{1}H-NMR	7.24-8.32(a)	C-H(Aromatic)	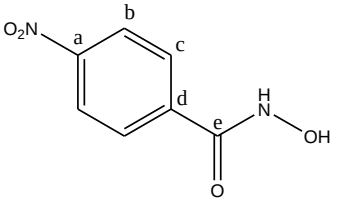
	9.28 (b)	O-H	
^{13}C-NMR	124.23 131.21	C=C(Aromatic)	
	136.76	C(d)	
	150.47	C-NO_2	
	166.37(c)	C=O	
^{1}H-NMR	7.24-8.32(a)	Aromatic	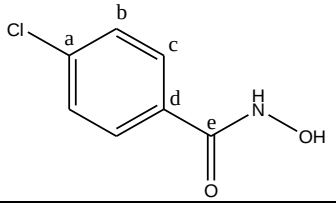

Meanwhile, a weak absorption peak at 379 nm depicted the n→π^* transition which specified the presence of carbonyl group in the ligand structure. There was an absorption peak at 290 nm in hydroxylamine hydrochloride which symbolized the n→σ*. This happened due to the presence of lone pair electrons in nitrogen and oxygen atoms of the ligand.

4. Nuclear Magnetic Resonance

Table 4 shows the ^{13}C and ^{1}H-NMR data for the ligands and data compatible with the proposed structures of the ligands, as recommended. The signals were obtained by using DMSO as solvent. The signals that appeared in the spectra were compatible with the structures. The presence of singlet broad peaks at the downfield regions, which were at 9.28 ppm (4NBHA) and 9.51 ppm (4CBHA), represented the OH proton. Irshad *et al*. (2018) [9] stated that the downfield shifting of OH proton showed the presence of intermolecular hydrogen bonding between hydroxy proton and oxygen of carbonyl group. Sandeep and Suryaprakash (2017) reported that the NH proton peak can disappear due to NH proton chemical exchange or by the property of nitrogen atoms, called quadrupole broadening. Besides, there was a multiplet peak which appeared in the chemical shift of 8 ppm – 9 ppm, which represented the aromatic protons. According to Naqeebullah (2014) [10], the proton signal appeared with an integration equivalent to four protons which were attached to each carbon. The slow relaxation time of the ^{13}C-NMR (4CBHA) caused the carbon peaks to disappear. In the ^{13}C-NMR of 4NBHA, the aromatic carbon was displayed at 124.23 ppm – 150.47 ppm and C=O ketone was observed at a downfield peak, which was at 166.37 ppm. The aromatic peaks appeared at downfield because of the resonance and anisotropic effect in cyclic π-system. Meanwhile, for the ketone, the presence of electronegativity atoms made the carbon deshielded and shifted to the downfield because of electron density reduction around the proton and carbon.

5. Corrosion Inhibition Study

In this study, the ligands were tested to observe their efficiency to reduce the corrosion rate of mild steel at different inhibitor concentrations. Five different concentrations of the ligands as inhibitor were used (0.001 M, 0.002 M, 0.003 M, 0.004 M and 0.005 M). Moreover, the acid without inhibitor was used as a blank for reference. The weight loss of mild steel was calculated by difference in initial mass and final mass of mild steel. The value of mass loss was used to define the corrosion rate of each concentration of inhibitors by using Equation 3. The effectiveness percentage of the ligands as inhibitor toward mild steel corrosion was calculated based on mass loss values to represent the corrosion rate. The mass loss method was studied at room temperature for a twenty-four-hour immersion process. The mass loss (ΔW), corrosion rate (C_{RW}), and inhibitor efficiency (% η_w) were calculated based on Equations 1, 2, and 3, respectively.

$$\Delta W = W_1 - W_2 \qquad \text{Equation 1}$$

$$C_{RW} = \frac{\Delta W}{s \times t} \qquad \text{Equation 2}$$

$$\% \eta_w = \frac{C°_{RW} - C_{RW} \times 100\%}{C°_{RW}} \qquad \text{Equation 3}$$

Where :

W_1= The average mass of mild steel before immersion (g)

W_2= The average mass of mild steel after immersion (g)
ΔW= The average mass loss (g)
s = The surface area of mild steel (cm^2)
t = The immersion time
$C°_{RW}$ = The corrosion rate in the absence of inhibitor
C_{RW} = The corrosion rate in the presence of inhibitor
% η_w = Inhibitor efficiency

From the results in Table 5, Figure 6, and Figure 7, the corrosion rate of the mild steel decreased as the concentration of the inhibitors increased. This was due to the presence of lone pair electrons from the heteroatoms, O and N in the ligand structures which were adsorbed onto the surface of the mild steel to protect the mild steel from corrosion [11,12]. The inhibition efficiency was better at higher concentration for 4CBHA as compared to 4NBHA. According to El-Maksoud (2008) [13], the halide ion in 4CBHA facilitated the adsorption of cation on the mild steel surface which formed intermediate bridges that were oriented toward the solution and mild steel. Eventually this could enhance the effectiveness of the corrosion inhibitor. Nitro, NO_2 and chloro, Cl substituents are attached at the same position in an aromatic ring which is a para position. The nitro group is a strong withdrawing group as compared to the chloro group.

Table 5. Corrosion inhibition data for ligands in H_2SO_4

Inhibitor	Concentration (M)	Weight loss, ΔW (g)	Corrosion rates, C_{Rw} (g cm^{-1} h^{-1})	Inhibitor efficiency, η_w (%)
Blank	0.000	0.130	1.44 × 10-3	0
4NBHA	0.001	0.075	8.33 × 10-4	42.20
	0.002	0.052	5.78 × 10-4	60.00
	0.003	0.034	3.78 × 10-4	73.80
	0.004	0.032	3.56 × 10-4	75.30
	0.005	0.029	3.22 × 10-4	77.60
4CBHA	0.001	0.060	6.66 × 10-4	53.75
	0.002	0.050	5.55 × 10-4	61.46
	0.003	0.030	3.33 × 10-4	76.87
	0.004	0.028	3.11 × 10-4	78.40
	0.005	0.025	2.77 × 10-4	80.76

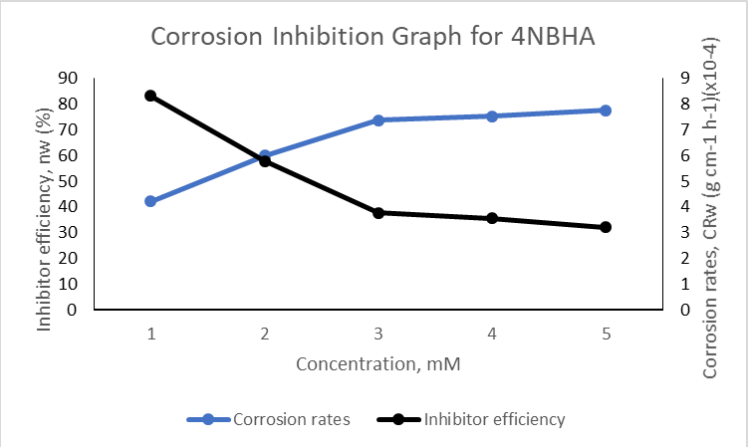

Figure 6. Corrosion rate and inhibitor efficiency in different concentrations of 4NBHA in H_2SO_4

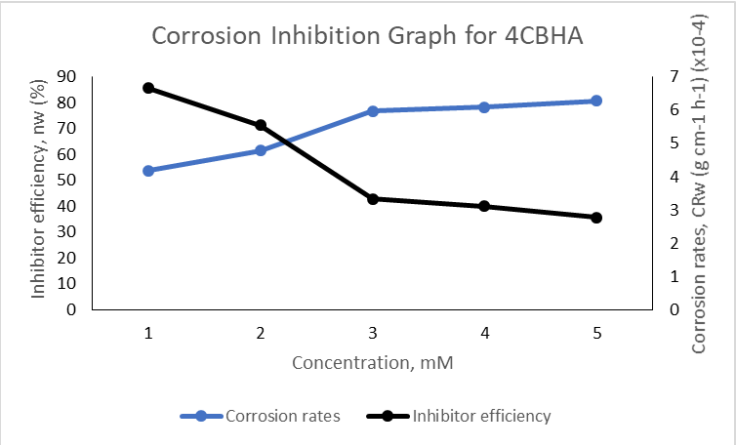

Figure 7. Corrosion rate and inhibitor efficiency in different concentration of 4CBHA in H_2SO_4

Hence, the nitro group will deactivate the aromatic ring more at para position as compared to the chloro group by lessening the electron density through the resonance withdrawing effect [14, 15]. Besides, the adsorption of inhibitor through π electrons of the aromatic ring and electron pair of N and O on the mild steel may decrease the anodic dissolution site. The adsorption mechanism occurs by electrostatic attraction between inhibitor and charged metallic ions of mild steel.

6. Adsorption Isotherm Study

Langmuir adsorption isotherms as shown in Figures 8 and 9 were used to explain the best isotherm to determine the adsorption process. The adsorption isotherm specified the crucial evidence in regard to the nature of inhibitor-mild steel interaction. Langmuir isotherm calculation was well-suited with the corrosion rate values obtained from the weight loss study. The degree of surface coverage (Θ) attained from the weight loss study was used to classify the best type of adsorption isotherm that fits into the corrosion rate values obtained. The degree of surface coverage(Θ) was calculated by using Equation 4:

$$\theta = \frac{W^0 corr - Wcorr}{Wcorr} \qquad \text{Equation 4}$$

Where, W_{corr} and W^0_{corr} are the corrosion rates of mild steel with and without the inhibitor, respectively [16]. The surface coverage, Θ values are very helpful in explaining the adsorption characteristic. The surface coverage on the mild steel was related to the concentration of inhibitor at a constant temperature and was graphically certified by fitting into the Langmuir Isotherm. From the equation, K_{ads} is the equilibrium constant, C_{inh} is the concentration of inhibitor, and Θ is the degree of surface coverage calculated from Equation 4. According to the graph, the R^2 of 4NBHA was 0.9940 while for 4CBHA was 0.9914. The slopes showed the best correlation with the corrosion rate data of the inhibitors. The R^2 values supported that the ligands were adsorbed on the mild steel surface by forming a monolayer and there was no interaction between the adsorbed inhibitors [17].

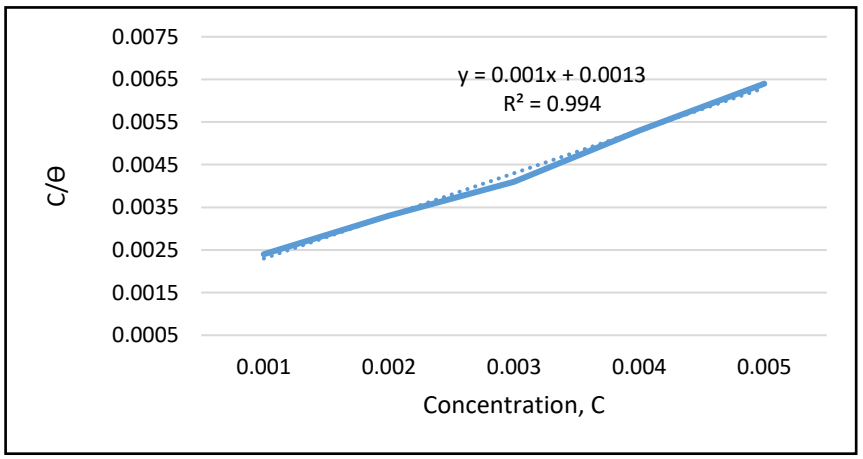

Figure 8. Graph of Langmuir isotherm of 4NBHA

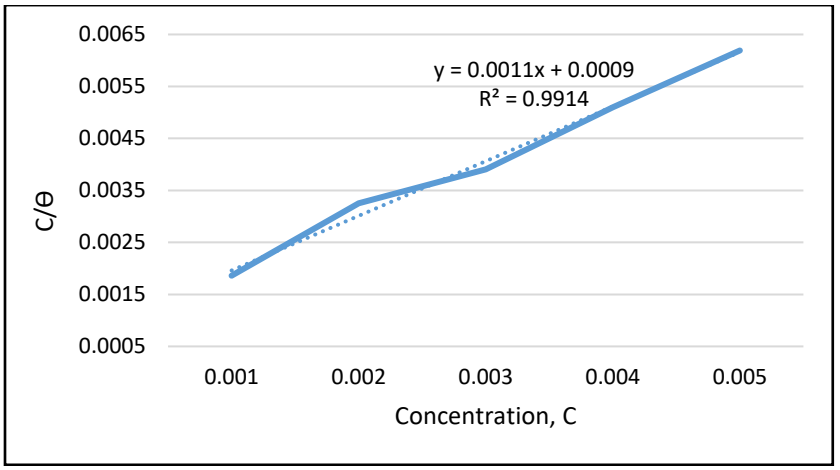

Figure 9. Graph of Langmuir isotherm of 4CBHA

Besides, the data proved that there was no chemisorption of uncharged inhibitors on the mild steel surface [18,19]. Sudhish and Eno (2011) [20] reported that inhibitors will be adsorbed on the mild steel surface if the interaction between them was higher than that of the water molecules and the mild steel surface.

7. Standard Free Energy (ΔG_{ads})

The values of activation energy for mild steel corrosion reaction were obtained from the Arrhenius equation. Standard free energy of adsorption (ΔG_{ads}) can be calculated by using the following equation:

$$\Delta G_{ads} = -RTln(K_{ads} \times A)$$

R = gas constant (8.314 $JK^{-1}mol^{-1}$)

A = water density (1000 g/L)

T = Temperature (K)

K_{ads} = adsorption equilibrium constant

The values of ΔG_{ads} obtained from the calculation were -43.55 $kJmol^{-1}$ (4NBHA) and -44.46 $kJmol^{-1}$ (4CBHA). This showed that the ligands were adsorbed by chemisorption onto the mild steel surface by the adsorption of heteroatoms, such as oxygen, nitrogen, sulphur, and phosphorus [21,22]. The negative value of ΔG_{ads} revealed that the adsorption process of inhibitor on the mild steel was by a spontaneous nature. Obot *et al*. 2013 [23] reported that the positive value of ΔG_{ads}, endothermic reaction referred to chemisorption while the negative value of ΔG_{ads}, the exothermic reaction referred to physisorption. Chemisorptions also happened when there was a transfer or sharing of inhibitor to mild steel to form a coordinate type of bond [24]. The values of ΔG_{ads} lower than -20 $kJmol^{-1}$ were physisorption and the values lower than -40 $kJmol^{-1}$ were chemisorption which involved the sharing of electrons from the inhibitor to the mild steel surface to form a chemical bond [24].

8. FESEM Analysis

The FESEM analysis was performed to study the mild steel surface in the absence and presence of the inhibitors. Figure 10 shows the surface of the mild steel with or without inhibitor at magnification of 2500×. Figure 10(a) shows the absence of corrosion due to the smooth surface of the mild steel. In Figure 10(b) there is a huge corrosion site on the surface of the mild steel, which was due to the acid attack of H_2SO_4 on the mild steel. From Figures 10(c) and (d), the images show that the surface of the mild steel is smooth and there is formation of a protective layer on the surface of the mild steel. The protective layer eventually inhibited the acid media which attacked the mild steel surface.

Table 6 shows the elemental compositions present on the surface of the mild steel. The main element in each mild steel was iron. For Figure 10(c), the mild steel contained nitrogen which showed the presence of 4NBHA as a protective layer to avoid corrosion. Figure 10(d) shows the mild steel which contained chloride, indicating the presence of 4CBHA as the protective layer. Therefore, it was evident that the inhibitors offered protection from corrosion on the mild steel surfaces.

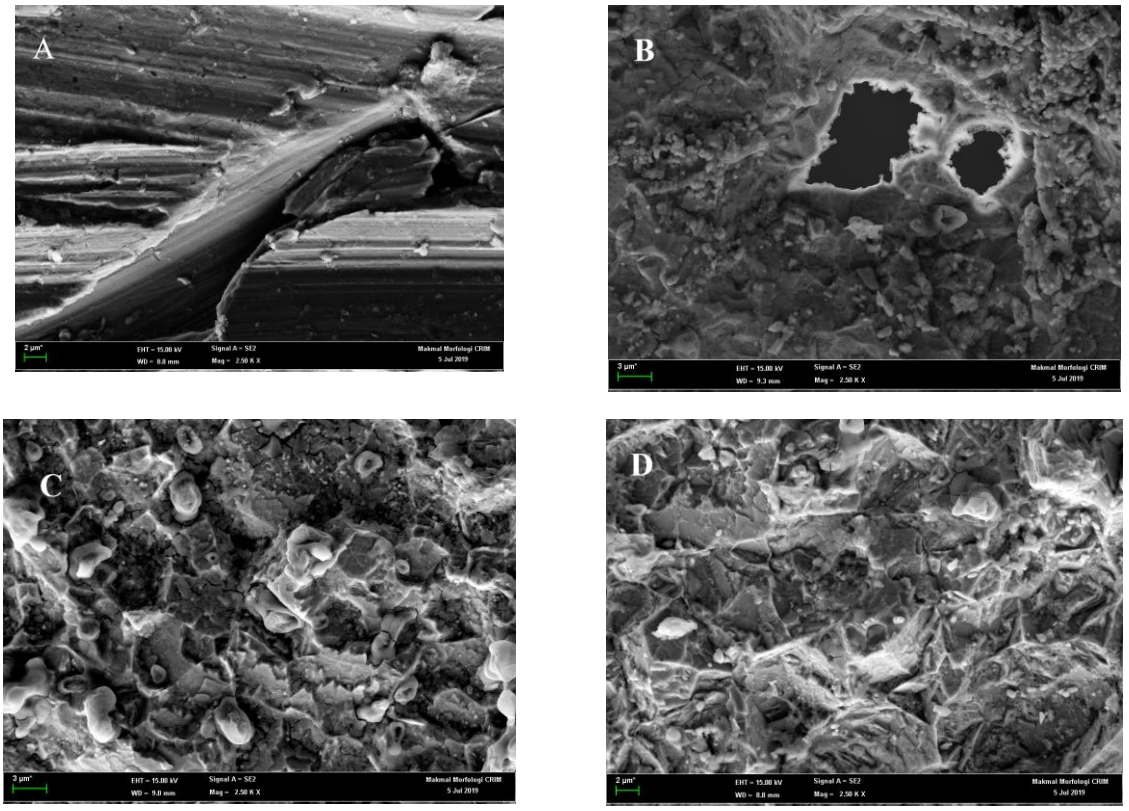

Figure 10. FESEM images of mild steel surface: (a) polished, (b) immersed in 1 M H_2SO_4 for 24 h, (c) immersed in 1 M H_2SO_4 with 4NBHA for 24 h (d) immersed in 1 M H_2SO_4 with 4CBHA for 24 h.

Table 6. The compositions of mild steel in the presence and absence of inhibitors in 1 M H_2SO_4

Inhibitors	Compositions					
	Fe	C	O	S	N	Cl
Polished Mild steel	85.9	7.8	-	-	-	-
Mild steel with 1 M H_2SO_4	81.5	6.9	1.1	0.7	-	-
Mild steel with 1 M H_2SO_4 and 4NBHA	87.5	5.0	6.6	0.4	0.4	-
Mild steel with 1 M H_2SO_4 and 4CBHA	90	4.6	5.1	-	0.2	0.1

CONCLUSION

The ligands, 4NBHA and 4CBHA were successfully synthesized and characterized by using FTIR-ATR, UV-Vis, and NMR spectroscopies. From the weight loss analysis, the ligands showed good inhibition efficiency against corrosion of mild steel by using different concentrations of ligands. Higher concentrations of the inhibitors showed better efficiency of the inhibitors against corrosion on the mild steel for both ligands. Since the corrosion process was inhibited by the adsorption of the inhibitors on the mild steel surface, it followed the Langmuir's adsorption isotherm. The negative values of ΔG_{ads} obtained indicated that the ligands were spontaneously adsorbed on the mild steel surface through the chemisorption process. The FESEM analysis showed that the mild steel which had an inhibitor on it had a protective layer which helped the mild steel to inhibit corrosion activity.

ACKNOWLEDGEMENT

The authors would like to express their gratitude to the Faculty of Applied Sciences, Universiti Teknologi MARA, Negeri Sembilan Branch, Kuala Pilah Campus, Negeri Sembilan, Malaysia for providing the research facilities.

REFERENCES

1. Solmaz, R. (2014) Investigation of corrosion inhibition mechanism and stability of Vitamin B1 on mild steel in 0.5 M HCl solution, *Corrosion Science*, **81**, 75–84.

2. Nassar, A. M., Hassan, A. M., Shoeib, M. A. and El-Kmash, A. N. (2015) Synthesis, characterization and anticorrosion studies of new homobimetallic Co(II), Ni(II), Cu(II) and Zn(II) Schiff base complexes, *Journal of Bio- and Tribo-Corrosion*, **1(3)**,19–34.

3. Alagta, A. R. (2009) Investigation of carbon steel corrosion inhibition by hydroxamic acids, *Material Science Forum*, **41(1)**, 527–538.

4. Graisa, A., Farina, Y., Yousif, E. and Kassem, M. (2008) Synthesis and Characterization of Some Organotin(IV) Complexes of *N*-Tolyl-*m*-nitrobenzohydroxamic acid, *ARPN Journal of Engineering and Applied Sciences*, **3(6)**, 47–50.

5. Hope, G. A., Woods, R., Buckley, A. N., White, J. M. and McLean, J. (2010) Spectroscopic characterisation of *N*-octanohydroxamic acid and potassium hydrogen *N*-octanohydroxamate, *Inorganica Chimica Acta*, **363(5)**,935–943.

6. Naqeebullah, K., Farina, Y., Mun, L. K., Rajab, N. F. and Awang, N. (2013) Spectral characterization and crystal structures of two newly synthesized ligands of *N*-methyl *O*-substituted benzohydroxamic acids, *Journal of Chemical Crystallography*, **43(11)**, 622–627.

7. Sandeep, K. M. and Suryaprakash, N. (2017) Intramolecular Hydrogen Bonding Involving Organic Fluorine: NMR Investigations Corroborated by DFT-Based Theoretical Calculations, *Molecules*, **22(3)**, 1–41.

8. Lewis, N. A., Liu, F., Seymour, L., Magnusen, A., Erves, T. R., Arca, J. F., Beckford, F. A., Venkatraman, R., Gonzalez-Sarrias, A., Fronczek, F. R., Vanderveer, D. G., Seeram, N. P., Liu, A., Jarrett, W. L. and Holder, A. A. (2012) Sythesis, characterisation, and preliminary in vitro studies of Vanadium(IV) complexes with a Schiff Base and thiosemicarbazones as mixed ligands, *European Journal of Inorganic Chemistry*, **4**, 664–677.

9. Irshad, A., Khan, N., Farina, Y., Baloch, N., Ali, A., Mun, L. K. and Murtaza, G. (2018) Synthesis, spectroscopic characterization, X-ray diffraction studies and in-vitro antibacterial activities of diorganotin(IV) derivatives with *N*-methyl-4-bromobenzohydroxamic acid, *Inorganica Chimica Acta*, **469**, 280–287.

10. Naqeebullah, K., Farina, Y., Mun, L. K., Rajab, N. F. and Awang, N. (2014) Triorganotin(IV) complexes with O-substituted arylhydroxamates: Synthesis, spectroscopic characterization, X-ray structures and in vitro cytotoxic activities, *Journal of Organometallic Chemistry*, **763**, 26–33.

11. Amitha Rani, B. E. and Basu, B. B. J. (2012) Green inhibitors for corrosion protection of metals and alloys: An overview, *International Journal of corrosion*, **2012**, 1–15.

12. Salima, K. A., Wassan, B. A. and Anees, A. K. (2019) Synthesis and investigations of heterocyclic compounds as corrosion inhibitors for mild steel in hydrochloric acid, *International Journal of Industrial Chemistry*, **10(2)**,159–173.

13. El-Maksoud, S. A. (2008) The effect of organic compounds on the electrochemical behaviour of steel in acidic media, *A review: International Journal of Electrochemical Science*, **3(5)**, 528–555.

14. Ghani, A. A., Bahron, H., Harun, M. K. and Kassim, K. (2016) Substituent Effect on Corrosion Inhibition of Schiff Bases Derived from Isatin, *Scientific Research Journal*, **13**(**1)**, 1–14.

15. Verma, C., Quraishi, M. A. and Ebenso, E. E. (2018) Microwave and ultrasound irridations for the synthesis of environmentally sustainable corrosion inhibitors: An overview, *Sustainable Chemistry and Pharmacy*, **10**, 134–147.

16. Ashassi-Sorkhabi, H., Shaabani, B. and Seifzadeh, D. (2005) Corrosion inhibition of mild steel by some Schiff base compounds in hydrochloric acid, *Applied Surface Science*, **239(2**), 154–164.

17. Aisha, A.G. (2019) Comparative Evaluation of Anticorrosive Properties of Mahaleb Seed Extract on Carbon Steel in Two Acidic Solutions, *Materials*, **12**, 3013–3031.

18. Hosseini, M., Mertens, S. F., Ghorbani, M. and Arshadi, M. R. (2003) Asymmetrical Schiff bases as inhibitors of mild steel corrosion in sulphuric acid media. *Materials Chemistry and Physics*, **78(3)**, 800–808.

19. Al-Fakih, A. M., Aziz, M. and Sirat, H. M. (2015) Turmeric and ginger as green inhibitors of mild steel corrosion in acidic medium, *Journal of Material Environment Science*, **6(5)**,1480–1487.

20. Sudhish, K. S. and Eno, E. E. (2011) Corrosion Inhibition, Adsorption Behavior and Thermodynamic Properties of Streptomycin on Mild Steel in Hydrochloric Acid Medium, *International Journal of Electrochemical Science*, **6**, 3277–3291.

21. Singh, A. K. and Quraishi, M. A. (2010) Effect of Cefazolin on the corrosion of mild steel in HCl solution, *Corrosion Science*, **52(1)**, 152–160.

22. Karthikaiselvi, R. and Subhashini, S. (2014) Study of adsorption properties and inhibition of mild steel corrosion in hydrochloric acid media by water soluble composite poly(vinyl alcohol-*O*-methoxy aniline), *Journal of the Association of Arab Universities for Basic and Applied Sciences*, **16**, 74–82.

23. Obot, I. B., Ebenso, E. E. and Kabanda, M. M. (2013) Metronidazole as Environmentally Safe Corrosion Inhibitor for Mild Steel in 0.5 M HCl: Experimental and Theoretical Investigation, *Journal of Environmental Chemical Engineering*, **1**, 431–439.

24. Hazani, N. N., Mohd, Y., Ghazali, S. A. I. S. M., Farina, Y. and Dzulkifli, N. N. (2019) Electrochemical Studies on Corrosion Inhibition Behaviour of Synthesised 2-acetylpyridine 4-ethyl-3-thiosemicarbazone and Its Tin (IV) Complex for Mild Steel in 1 M HCl Solution, *Journal of Electrochemical Science and Technology*, **10(1)**, 29–36.